American Mineralogist, Volume 78, pages 804–818, 1993

Fluid infiltration through metachert layers at the contact aureole of the Bufa del Diente intrusion, northeast Mexico: Implications for wollastonite formation and fluid immiscibility

WILHELM HEINRICH
Institut für Angewandte Geophysik, Petrologie und Lagerstättenforschung, Technische Universität Berlin, EB 310, Straße des 17. Juni 135, 1000 Berlin 12, Germany

ABSTRACT

Cretaceous sediments were contact metamorphosed by the Tertiary Bufa del Diente alkali syenite. Within the massive impure limestones, an aureole developed with a tremolite, diopside, and wollastonite zone toward the contact. Numerous chert bands in the limestones extend several hundred meters from the contact. Broad wollastonite rims occur around the metachert layers into the tremolite zone. Isobaric ($P \approx 1000$ bars) univariant and invariant parageneses indicate that the fluid phase in the marbles was internally buffered and that the marbles were not subject to substantial aqueous fluid infiltration. In contrast, the metachert beds acted as channelways for H_2O-rich fluids under lithostatic pressure conditions. Fluid inclusions in recrystallized metachert quartz were studied from samples near the wollastonite isograd. Early highly saline brines [$T_h(V \rightarrow L) = 500$–$580$ °C, $T_m(\text{salt}) = 400$ °C, $(NaCl + KCl)_{eq} = 67$–73 wt%, K/Na ion ratios = 1–1.8] occur along the same microfractures as apparently one- or two-phase vapor-rich CO_2-bearing inclusions. The two fluids were simultaneously trapped in the two-fluid immiscibility field of the H_2O-CO_2-salt system at peak metamorphic conditions of 500–580 °C. Graphite-containing metacherts show similar features with highly saline brines coexisting with vapor-rich CH_4-bearing inclusions. Late brine populations have $T_h(V \rightarrow L) \approx T_m(\text{salt})$ ranging from 400 down to 150 °C. The K/Na ion ratios of the brines decrease from 1.8 to 0.3 as $T_h(V \rightarrow L)$ decreases from 580 to 150 °C. Trapping of brines channeled in the metacherts occurred continually from peak metamorphic conditions throughout the cooling history. Their compositions were controlled by mineral-fluid equilibria in the cooling alkali syenite reservoir. The low density CO_2-rich fluids were generated by the reaction calcite + quartz = wollastonite + CO_2 at the two-fluid solvus during flow of magmatic brine away from the heat source and probably escaped into the marble by grain-edge flow. The boundary between marble and wollastonite acted as a semipermeable membrane separating two flow patterns in the aureole.

INTRODUCTION

Contrasting fluid infiltration patterns through adjacent stratigraphic units in both regional-metamorphic and contact-metamorphic régimes (e.g., Hover-Granath et al., 1983; Nabelek et al., 1984; Ferry, 1987, 1988; Labotka et al., 1988) showed channeling of fluid flow along individual lithologic layers. In carbonate-rich metasediments, calcareous argillite beds and quartz-rich layers can act as aquifers, whereas impure limestones may be impermeable. In impervious units, equilibrium fluid compositions are internally buffered (Rice, 1977; Rice and Ferry, 1982) by prograde decarbonation and dehydration reactions and reflect the stoichiometric ratios of the volatile components evolved by the rocks. In contrast, there is a complex interplay between the compositions and volumes of evolved and infiltrated fluids in permeable beds (e.g., Rumble et al., 1982; Ferry, 1987; Labotka et al., 1988). Mass balance calculations give the amount and composition of fluids evolved during metamorphism. The amount of infiltrated fluid can be determined by comparing the composition of evolved fluids with the value of X_{CO_2} at equilibrium determined from mineral assemblages (Ferry, 1983, 1986, 1991). The results are time-integrated ratios of fluid to rock that can serve as fossil flux meters (Ferry, 1987). Models linking estimated fluid to rock ratios with heat and transport equations in porous media have been presented by Labotka et al. (1988) and Baumgartner and Ferry (1991). An important aspect is the direction of fluid flow. Labotka et al. (1988) suggested that decarbonation of pervious metaargillites at the Notch Peak aureole was driven by infiltrating fluids emanating from the intrusion. In contrast, Baumgartner and Ferry (1991) argued that mineral parageneses in equilibrium with infiltrating fluid are devolatilized by fluids flowing toward the heat source or toward the surface, whereas flow away from the heat source would result in hydration and carbonation of the rocks. Their model does not per-

0003–004X/93/0708–0804$02.00

mit decarbonation of calcareous beds by hot magmatic fluids unless decarbonation is not accompanied by a simultaneous pressure drop along with fluid flow. Consequently, Ferry and Dipple (1992) used the data of Labotka et al. (1988) to show flow paths in the opposite direction in the Notch Peak aureole.

The concept of fluid-rock ratios, calculated by the measured progress of devolatilization reactions is based on two strict assumptions: (1) local mineral and mineral-fluid equilibrium occurred everywhere in the flow system (Baumgartner and Ferry, 1991); (2) the corresponding devolatilization reactions proceeded when the coexisting H_2O-CO_2 fluid phase was homogeneous. Fluid inclusion studies in both contact-metamorphic and regional-metamorphic calcareous rocks (Sisson et al., 1981; Trommsdorff et al., 1985; Williams-Jones and Ferreira, 1989) confirmed that H_2O-CO_2 immiscibility can be caused at metamorphic conditions by the presence of dissolved salts and that decarbonation produced CO_2-rich fluid that might have escaped (Trommsdorff and Skippen, 1986). Bowers and Helgeson (1983a) and Trommsdorff and Skippen (1986) demonstrated the intense bearing on the development of prograde mineral reactions when the fluid-rock buffer system doesn't function because of CO_2 loss by effervescence.

This contribution presents a study of fluid infiltration through contact-metamorphic metachert layers at the Bufa del Diente intrusion, northeast Mexico, using petrographical and fluid inclusion observations. It will demonstrate that (1) fluid influx occurred in the direction of decreasing temperature along metachert layers, (2) local equilibrium was generally not maintained along metachert-marble boundaries, and (3) decarbonation proceeded in the two-fluid region of the H_2O-CO_2-salt system. Thus, boiling is driven by external fluid influx during pluton emplacement. Fluid flux in marbles is estimated by calculating the amount of low density CO_2-rich fluid lost into overlying marble.

Geological setting

The Bufa del Diente intrusion is part of the Tertiary Sierra de San Carlos alkaline igneous complex (Hubberten, 1985) located in Tamaulipas, northeast Mexico, about 180 km southeast from the city of Monterrey, Nuevo León, Mexico. The geology of the Bufa del Diente area has been described by Ramirez-Fernandez and Heinrich (1991). The Bufa del Diente stock is an ovoid-shaped alkali syenite that discordantly intruded undeformed Early to Late Cretaceous marine sedimentary rocks (Fig. 1). The strike of the beds is parallel to the strike of the contact, resulting in a dome structure. The sediments to the south of the stock, where the dip is shallower than to the north, were brought to a higher level, reflecting asymmetric magma emplacement. Outcrops in the area are perfectly exposed. Beds can be traced along the strike for several kilometers.

The Early Cretaceous Tamaulipas inferior and Tamaulipas superior Formations (Fig. 1) consist of thick-bedded

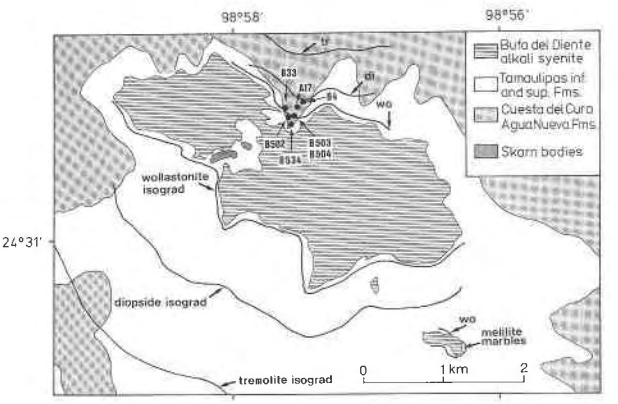

Fig. 1. Generalized geologic map of the Bufa del Diente area, simplified from Ramirez-Fernandez and Heinrich (1991), showing the Tertiary Bufa del Diente alkali syenite, the Upper Cretaceous Cuesta del Cura and Agua Nueva Formations, and the underlying Lower Cretaceous Tamaulipas superior and inferior Formations. Tremolite, diopside, and wollastonite isograds were mapped as occurring in the massive impure marbles. Black dots represent samples from interstratified metacherts and meta-argillites from Cuesta del Cura and Agua Nueva Formations. Numbers refer to sample numbers in the text.

micritic limestones. Interstratified calcareous argillites are rare and confined to the upper part of Tamaulipas superior Formation. Argillite-rich material is also present in stylolites. The overlying Late Cretaceous Cuesta del Cura Formation consists of limestones with chert nodules and numerous interstratified chert bands. Calcareous argillite beds occur in minor quantities. North of the aureole, individual chert strata are 4–15 cm thick. These can be traced for several hundred meters directly to their contact with the intrusion. At outcrops B502 and B503 there are some 50 individual chert beds across the Cuesta del Cura Formation, which is about 70 m thick. In the overlying Agua Nueva Formation, the number and thickness of calcareous argillite beds increase considerably. Toward the top of this formation, limestone and argillite layers have a similar thickness of about 30 cm.

This contribution focuses on the fluid evolution in the limestones as well as on metachert layers of the Cuesta del Cura Formation in a profile north of the Bufa del Diente stock (Fig. 1). The contact-metamorphic evolution of the calcareous argillites is considered elsewhere (Heinrich and Gottschalk, in preparation).

Mineral content of limestones

The progressive contact metamorphism of the impure limestones results in the successive appearance of tremolite, diopside, and wollastonite with decreasing distance to the contact (Fig. 1), resulting in four zones: calcite + dolomite + quartz (nonmetamorphic); calcite + tremolite + quartz (tremolite zone); calcite + diopside + quartz (diopside zone); and calcite + diopside + wollastonite (wollastonite zone). Since the limestones are relatively pure and dolomite deficient, calc-silicates rarely exceed

Table 1. Representative microprobe analyses of minerals from metamorphosed impure limestones (columns 1–6) and metachert layers (7–9) from Cuesta del Cura Formation

	Marbles						Metacherts		
Mineral	Tr	Tr	Phl	Di	Di	Kfs	Ri	Di in Ri	Pc
Zone	Tr	Tr	Tr	Di	Wo	Di			
No.	B19a7	B1282	B1261	B14-3	B11-3	B1104	B502-75	B502	B502-211
SiO_2	56.72	57.84	41.99	51.03	53.93	65.48	58.19	55.03	53.06
TiO_2	0.19	0.11	0.19	0.13	0.09	0.00	0.12	0.08	0.00
Al_2O_3	2.82	0.89	12.48	2.07	1.23	18.44	0.01	0.07	0.32
V_2O_3	0.00	0.00	0.00	0.00	0.00	0.00	0.08	2.25	0.00
Fe_2O_3	0.00	0.00	0.00	0.00	0.00	0.00	0.00	0.00	0.00
FeO	1.13	1.56	2.88	11.54	2.93	0.00	2.32	4.01	0.00
MnO	0.27	0.03	0.06	1.20	0.51	0.00	0.31	0.07	0.00
MgO	22.48	23.44	26.44	9.03	15.97	0.00	22.23	14.96	0.00
CaO	13.61	13.11	0.16	24.59	25.43	0.00	7.81	23.52	34.09
Na_2O	0.28	0.64	0.91	0.28	0.35	0.83	4.20	1.23	8.81
K_2O	0.23	0.05	8.98	0.00	0.00	14.99	3.63	0.00	0.01
F	0.26	0.17	0.09	0.00	0.00	0.00	3.91	0.00	0.00
O = F	0.11	0.07	0.04	0.00	0.00	0.00	1.65	0.00	0.00
Total	97.88	97.77	94.14	99.87	100.44	99.74	101.15	101.21	96.29
Cat*	23 O	23 O	11 O	6 O	6 O	8 O	23 O	6 O	8.5 O
Si	7.747	7.900	2.980	1.954	1.968	3.012	8.026	2.000	2.972
$^{[4]}Al$	0.253	0.100	1.020	0.046	0.032	—	—	—	0.021
$^{[6]}Al$	0.200	0.043	0.024	0.048	0.021	1.000	0.001	0.003	—
Ti	0.020	0.011	0.010	0.004	0.002	—	0.013	0.002	—
V^{3+}	—	—	—	—	—	—	0.009	0.066	—
Fe^{3+}	—	—	—	—	—	—	—	—	—
Fe^{2+}	0.130	0.178	0.171	0.370	0.090	—	0.268	0.122	—
Mn	0.031	0.003	0.004	0.039	0.016	—	0.036	0.002	—
Mg	4.577	4.773	2.798	0.516	0.869	—	4.571	0.810	—
Ca	1.991	1.917	0.012	1.009	0.994	—	1.153	0.916	2.045
Na	0.074	0.169	0.125	0.020	0.024	0.074	1.124	0.086	0.957
K	0.040	0.009	0.813	—	—	0.880	0.638	—	0.001
Total	15.063	15.103	7.975	4.006	4.016	4.966	15.839	4.007	5.996

Note: Ri = richterite; Pc = pectolite.
* Cations on the basis of O atoms.

10% of the rocks' mode. Talc- and forsterite-bearing assemblages were not detected. Alkali feldspar and phlogopite are occasionally present. Representative mineral analyses are given in Table 1. Within the mineral zones, isobaric univariant assemblages in the CaO-MgO-SiO_2-CO_2-H_2O system are common and the isobaric invariant assemblage dolomite + calcite + quartz + tremolite + diopside was detected at several locations close to the diopside isograd.

The asymmetry of the magma emplacement is reflected in the greater width of the tremolite and diopside zones south of the intrusion. In the north, the tremolite and diopside isograds are closer to the contact than in the south, reflecting a steeper dip in the north (Ramirez-Fernandez and Heinrich, 1991).

Mineral content of metacherts

The progressive contact metamorphism of the chert layers of the Cuesta del Cura Formation resulted in the extensive formation of wollastonite according to the reaction calcite + quartz = wollastonite + CO_2 along the chert-marble boundaries. Wollastonite rims along chert layers occur at the contact with the intrusion and extend far into the diopside zone. Some wollastonite rims were found in the tremolite zone, at a distance of >400 m from the contact. Wollastonite either may form as rims on both sides of the chert-marble boundary or may separate the chert band into rounded quartzite nodules (Fig. 2A). The thickness of the rims correlates roughly with decreasing distance from the contact. It is generally not related to the thickness of the metachert bands. Typically, in the wollastonite zone, chert layers of 4–6 cm thickness are completely reacted, resulting in pure wollastonite bands. In adjacent layers, 10–15 cm thick, thin quartzite bands or nodules remained. However, there are exceptions to this, as rare metacherts with thin wollastonite rims near the contact and others with thick rims exist in the diopside zone. A rough estimate based on the rim thickness of some 50 individual layers gives an average of about 3 cm^3 wollastonite to 1 cm^2 metachert layer at the wollastonite isograd, 2 cm^3/cm^2 at the central diopside zone, and 0.3 cm^3/cm^2 near the diopside isograd (outcrops B502, A17, B4, respectively, in Fig. 1).

Thin pegmatitic veins are common and can be traced up to 100 m from the contact to the wollastonite isograd. They are confined exclusively to the metachert layers and are strictly conformable with bedding. Moreover, pegmatitic veins only occur along one of the two quartz-wollastonite boundaries (Fig. 2B), indicating that vein crystallization took place after wollastonite formation. Pegmatitic veins were not observed along wollastonite-marble boundaries. It is emphasized that vertical peg-

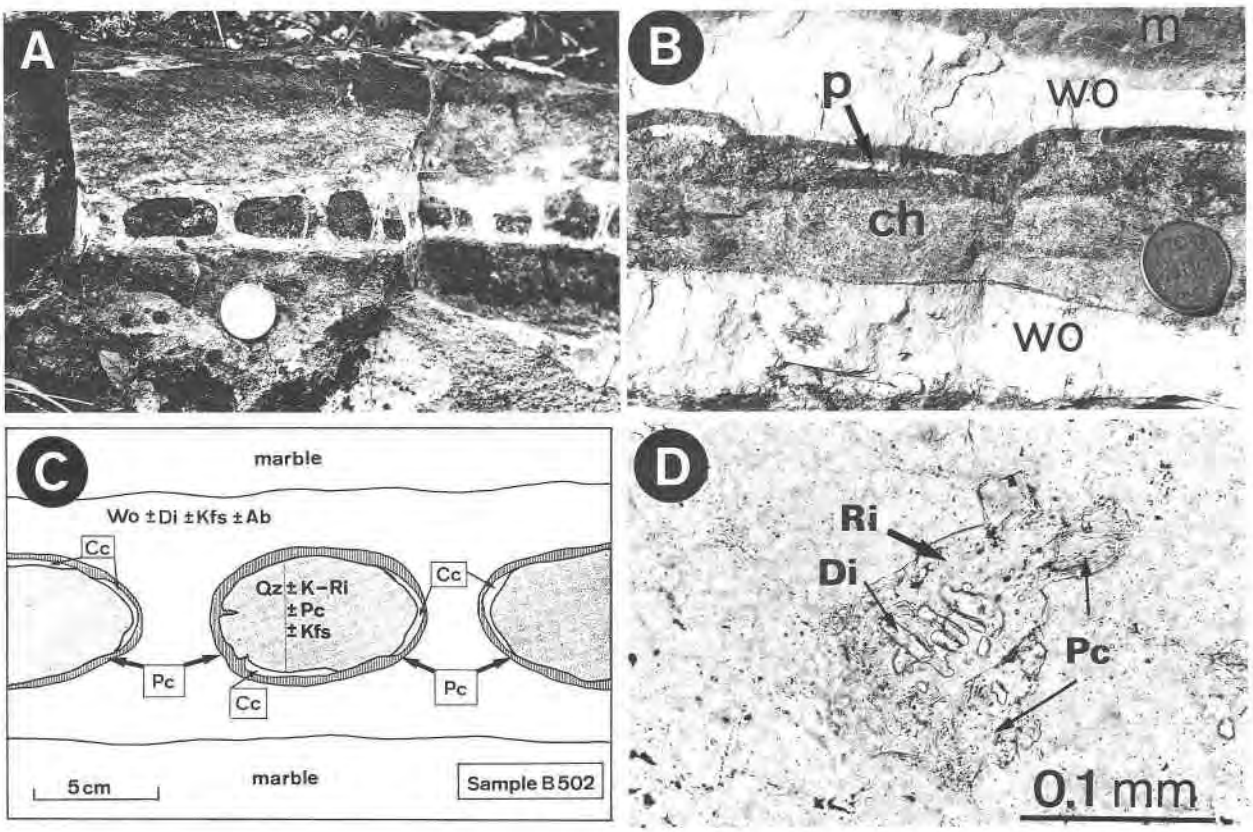

Fig. 2. (**A**) Wollastonite-rimmed metachert band embedded in diopside-zone marble from Agua Nueva Formation (Sample A17). (**B**) Wollastonite-rimmed (wo) metachert band (ch) embedded in marble (m) from the boundary between the diopside and wollastonite zones, Cuesta del Cura Formation. A pegmatitic vein (p) consisting of acmite rims (dark), perthitic alkali feldspars (white), and eudialyte is strictly comformable with bedding and separates the upper wollastonite-quartz border along a distance >60 m from the contact. (Sample B33, graphite-free). (**C**) Sketch of graphite-free metachert sample B502 from the diopside-wollastonite boundary. The wollastonite rim contains minor amounts of diopside (Di), alkali feldspar (Kfs), and albite (Ab). Remaining quartz nodules are recrystallized and associated with K-rich richterite (K-Ri), pectolite (Pc), and Kfs. They are themselves rimmed by calcite (Cc) and Pc. (**D**) Detail from **C**: K-rich richterite (Ri) with inclusions of diopside and pectolite.

matitic or hydrothermal vein systems in the Cuesta del Cura Formation do not exist. There is no field indication of any vertical fluid or mass transport by fractures at this level of the aureole.

The wollastonite rims of the metacherts may include accessories such as alkali feldspar, albite, plagioclase (An_{15-27}), diopside, titanite, Na-rich chlorine scapolite, vesuvianite, and grandite solid solutions, reflecting the low argillite content of the chert protolith. These minor phases form very thin (commonly ≤ 1 mm) margins at the wollastonite-marble boundaries and at most make up a few percent of the metacherts' modal content. Thus, the reaction calcite + quartz = wollastonite + CO_2 accounts almost exclusively for the CO_2 produced in the metachert layers.

The metacherts far from the contact are rich in organic material. Graphite occurs up to about the wollastonite isograd. From there to the contact, metacherts are bleached and are generally graphite-free. However, occasionally graphite persists up to the contact. Wollastonite rims are free of graphite throughout the profile. Bleaching is accompanied by significant quartz recrystallization from grains ≤ 0.1 mm in the diopside zone to grain sizes around 1 mm beyond the wollastonite isograd.

Remaining quartz nodules are themselves rimmed by thin pectolite ($NaHCa_2Si_3O_9$, Table 1) and calcite assemblages (Fig. 2C). This can be observed at quartzite-wollastonite boundaries throughout the profiles. Pectolite also occurs inside the quartzite nodules along with small amounts of diopside and alkali feldspar and traces of fluorite (Fig. 2C). Throughout the wollastonite zone, alkali-rich amphibole solid solutions occur inside the metacherts. These amphiboles typically enclose previously formed contact-metamorphic diopside (Fig. 2D). They are Al-free and F-rich (Table 1). Cl was not detected. Amphibole solid solutions have compositions of 60–70 mol% potassium richterite, 20–40 mol% richterite, and 0–20 mol% tremolite component.

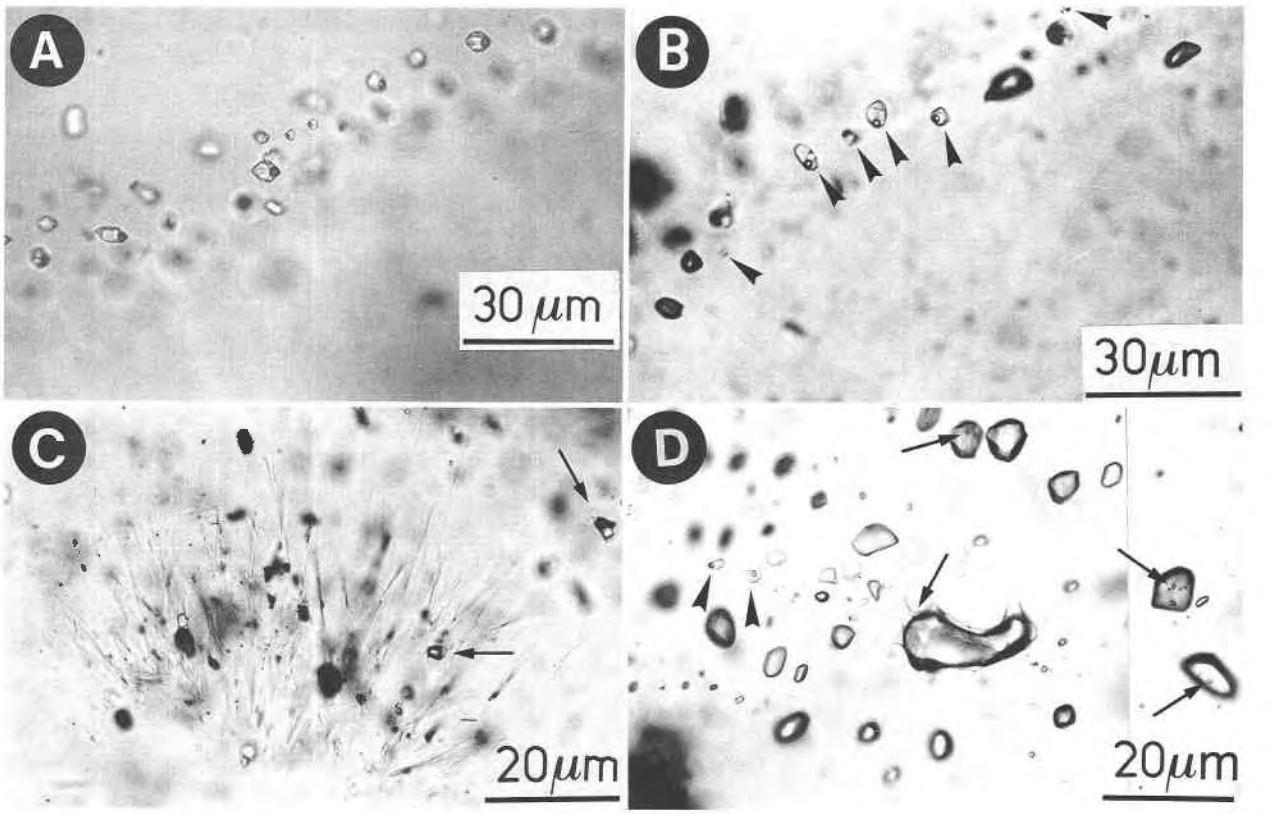

Fig. 3. Fluid inclusions in recrystallized quartz from metacherts from the diopside-wollastonite boundary. (**A**) Sample B502. Typical H_2O-rich highly saline four-phase fluid inclusions with a big sylvite and a smaller halite crystal exhibiting similar crystal forms and phase relations. (**B**) Sample B502. H_2O-rich highly saline four-phase fluid inclusions (arrows) occurring along the same trail as apparently one-phase vapor-rich CO_2-bearing inclusions. (**C**) Sample B502. H_2O-rich highly saline and vapor-rich CO_2 inclusions (arrows) associated with thin wollastonite needles growing into quartz crystal. Vapor-rich inclusions reveal varying phase relations indicative of heterogeneous trapping of the two coexisting fluids. (**D**) Methane-rich fluid inclusions in graphite-containing metachert sample B503. They are apparently monophase (vapor) or two-phase (liquid + vapor) at room temperature. Some of these inclusions additionally contain one or more salt crystals (long arrows), though often a liquid phase is not visible. H_2O-rich highly saline four-phase inclusions are denoted by short arrows.

Fluid inclusions

Petrography

Fluid inclusions were studied in recrystallized quartzite nodules from four samples: B502, B33, B503, and B504, all taken from near the boundary between the diopside and wollastonite zones (Fig. 1). Only a few inclusions were observed in wollastonite from the associated rims. Sample B502 is graphite-free, B33 is graphite-free and associated with a pegmatitic vein (Fig. 2B), and B503 and B504 are graphite-bearing. Quartz recrystallization in the diopside- and tremolite-zone metacherts was minor, and the fluid inclusions trapped in these zones were too small (≤ 2 μm) for reasonable fluid inclusion measurements.

Samples B502 and B33 are extremely rich in fluid inclusions, consisting predominantly of highly saline four-phase H_2O-rich inclusions with a large sylvite crystal, a smaller halite daughter crystal, and a small vapor bubble at room temperature (Fig. 3A). The inclusions are <10 μm in diameter. They were trapped mainly along healed microfractures and clusters and are considered to be of secondary origin. There is no unequivocal evidence of primary or pseudosecondary inclusions. Individual inclusions along a distinct trail generally exhibit similar negative crystal forms and identical phase relations (Fig. 3A), thus defining a fluid inclusion population. A single quartz grain of 1 mm in size may be cut by up to 20 populations. These differ at room temperature, especially in the characteristic sizes of the daughter crystals. Populations with smaller salt crystals as shown in Figure 3 are common. There are H_2O-rich two-phase populations without daughter crystals. However, freezing and heating cycles showed that daughter crystals are absent metastably up to salinities of 42 wt% $(NaCl + KCl)_{eq}$. This might be an effect of fast heating and cooling during sample preparation (Sterner et al., 1988). In any case, H_2O-rich halite-undersaturated fluid inclusions are not present in these rocks. Crosscutting relationships between the distinct

population trails and between trails and quartz grain boundaries suggest a chronological sequence throughout the samples. Very highly saline populations formed early, whereas populations with lower salinity developed later.

In samples B502 and B33, a second type, consisting of vapor-rich CO_2-bearing inclusions, occurs. These are extremely rare and at room temperature apparently one phase; sometimes a small amount of H_2O is visible. Daughter crystals are not present. Sizes are typically 5–10 μm and do not exceed 12 μm. These inclusions are always associated with highly saline H_2O-rich inclusions. Figure 3B shows that apparently one-phase vapor-rich CO_2-bearing inclusions exist along the same microfractures as highly saline four-phase inclusions. From a textural standpoint these inclusions were simultaneously trapped in the two-fluid immiscibility field of the H_2O-CO_2-salt system (Gehrig, 1980; Bowers and Helgeson, 1983b; Trommsdorff and Skippen, 1986). Trapping was largely homogeneous for both fluid types, which is a rare case (Ramboz et al., 1982). However, there is also textural evidence for heterogeneous trapping, resulting in trails with variable degrees of filling and also in the formation of vapor-rich CO_2-bearing inclusions containing salt crystals, which indicate trapping of mixtures of the two immiscible fluids in various proportions (Ramboz et al., 1982). This is typically observed in rare fluid inclusion clusters that are associated with thin wollastonite needles growing into quartz crystals (Fig. 3C). Vapor-rich CO_2-bearing inclusions are rare, only appearing in about 3% of all highly saline populations. They represent about 0.01% of the total fluid inclusion population.

Fluid inclusions of the graphite-bearing samples B503 and B504 have H_2O-rich highly saline inclusion populations. Likewise, halite-undersaturated H_2O-rich inclusions do not occur. However, these samples contain many vapor-rich, apparently one- or two-phase, CH_4-bearing inclusions, often forming negative crystals to 40 μm. Their textural relationships with the highly saline inclusions are very similar to those described above, again indicating homogeneous as well as heterogeneous trapping of two immiscible fluids. Furthermore, these inclusions may also form separate trails and clusters not associated with highly saline inclusions. Some of the vapor-rich CH_4-bearing inclusions contain one or more salt crystals. Often no H_2O is visible (Fig. 3D). The relative proportion of the CH_4-bearing inclusions is about 40%. CO_2-bearing inclusions were not found in these samples.

Methods

Microthermometric data were obtained on a modified Linkam TH600 heating and freezing stage calibrated at the triple point of CO_2 (−56.6 °C), the triple point of H_2O (0 °C), the critical point of CO_2 (31.1 °C), and the critical point of H_2O (374.1 °C), using synthetic fluid inclusions synthesized hydrothermally at Fachgebiet Petrologie, TU Berlin. Temperature accuracy is ±0.3 °C at −56.6 °C, ±0.1 °C at 0 °C, ±0.1 °C at 31.1 °C, and ±4 °C at 374 °C, and is believed to be ±1 °C at −100 °C. Phase changes were repeated at least twice. Reproducibility is within the range of accuracy of the temperature determination.

Table 2. Leachate analyses of bulk fluid inclusion samples

Sample	Ion concentrations (ppm)				Ion ratios		
	Na	K	Mg	Ca	K/Na	Mg/Na	Ca/Na
B502/1	7.2	6.5	0.4	2.6	0.53	0.05	0.21
/2	3.5	3.6	0.29	8.6	0.60	0.08	1.41
/3	0.71	0.70	0.10	0.29	0.58	0.13	0.23
B33/1	3.7	0.9	0.55	5.4	0.14	0.14	0.84
/2	4.2	1.1	0.51	0.5	0.15	0.11	0.06
/3	2.1	0.8	0.19	0.23	0.22	0.09	0.06
B503/1	0.21	0.16	0.04	—	0.44	0.18	—
B504/1	3.6	2.8	0.24	—	0.61	0.10	—

Note: Results are averages of double determinations.

Partial chemical analyses of fluid inclusion leachates were obtained by crushing and leaching quartz grains from the quartzite nodules. Leachates were analyzed for K^+, Na^+, Mg^+, and Ca^{2+}, using standard AAS and ICP methods. The results presented in Table 2 are averages of double determinations.

Spectroscopic analyses of the constituent fluid species within fluid inclusions of samples B503 and B504 were done on a Ramanor U 1000 Raman microprobe equipped with an Ar ion laser (wavelength 514.5 nm).

Results

H_2O-rich highly saline inclusions. Results of 600 H_2O-rich highly saline fluid inclusions are presented in Figures 4 and 5. Data include only distinct inclusion populations with at least ten individual inclusions exhibiting similar phase relations. Any inclusions suspected of having been formed by heterogeneous trapping or by necking phenomena were excluded.

The salinities in these inclusions were determined using microthermometric data for the vapor-saturated system NaCl-KCl-H_2O (Sterner et al., 1988). Figure 4A shows the apparent KCl and NaCl contents of 214 inclusions of sample B502 as obtained by the final melting temperatures of KCl and NaCl in the presence of vapor. Data for 219 inclusions of sample B503 and of B504 cover an almost identical range. Final salt melting temperatures range continuously from 120 to 400 °C, resulting in total salinities from 33 to 73 wt% $(KCl + NaCl)_{eq}$. There is a good correlation between total salinity and the apparent KCl/(KCl + NaCl) ratios (wt%) with values from 0.69 to 0.29 as the total salinity decreases from 73 to 33 wt%. Recalculated bulk leachate analyses give average KCl/(KCl + NaCl) ratios (wt%) of 0.41–0.47 (Table 2). A similar trend is seen in sample B33 (Fig. 4B). NaCl final melting temperatures (90–390 °C) are almost identical to those of the other samples, although the KCl contents are significantly lower. KCl/(KCl + NaCl) ratios (wt%) range from 0.5 to values lower than 0.1 and roughly correlate with apparent total salinities of 58–≈30 wt% $(KCl + NaCl)_{eq}$. Average ratios from bulk leachate analyses have values from 0.14 to 0.22 (Table 2). In samples B502 and B503, the KCl contents at KCl/(KCl + NaCl) ratios <0.35

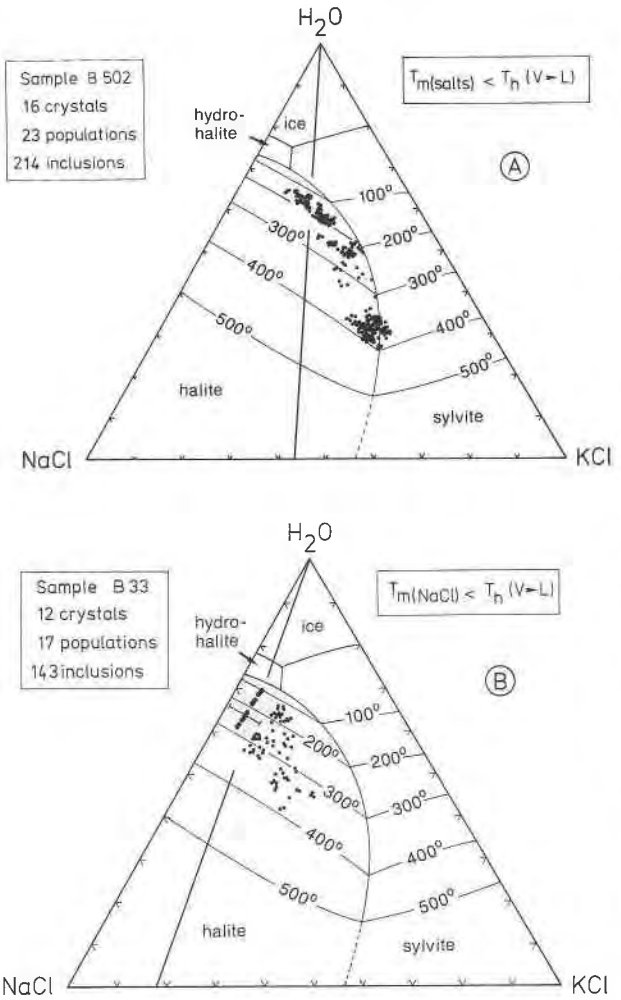

Fig. 4. Apparent NaCl and KCl contents of H_2O-rich four-phase fluid inclusions of samples B502 (**A**) and B33 (**B**) plotted on the vapor-saturated system NaCl-KCl-H_2O (Sterner et al., 1988). The thick line denotes the NaCl/KCl ratio calculated from bulk leachate analyses (Table 2). In B502, 23 inclusions have T_m(salts) $\geq$ T_h(V → L) and are not plotted in Fig. 5A (see Fig. 6A). For B33, at low KCl contents (shaded area) only NaCl final melting temperature is plotted. At this range, dots represent five individual inclusions. Scale bar gives the uncertainty range for KCl contents. For further explanation see text.

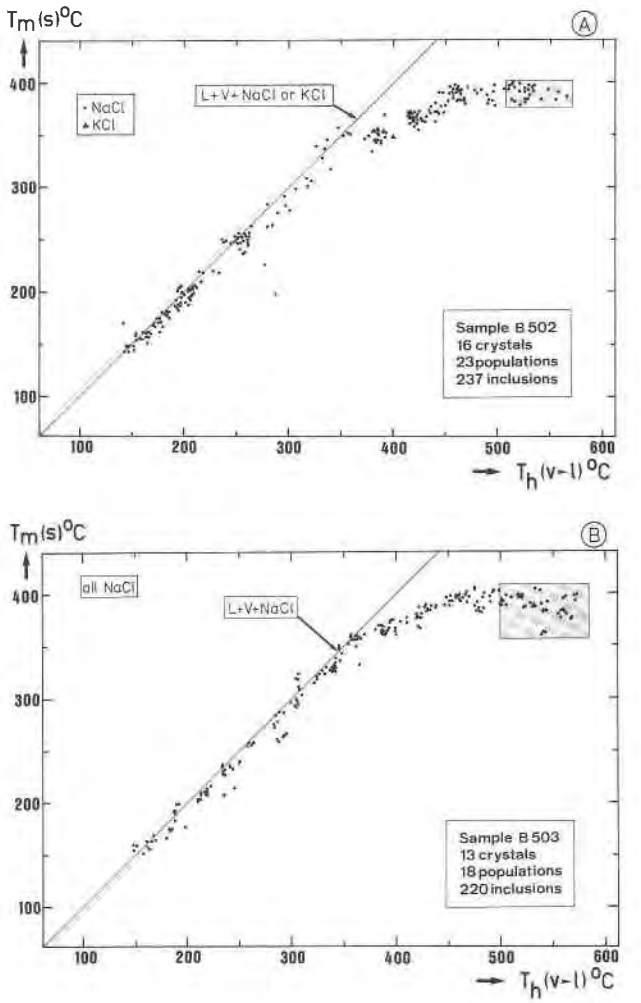

Fig. 5. Last salt melting temperature vs. total homogenization temperature of H_2O-rich highly saline four-phase inclusions of sample B 502 (**A**) and B503 (**B**). At T_h(V → L) between 500 and 580 °C (shaded area) many inclusions decrepitated before reaching homogenization.

are not well constrained because of metastable processes during freezing and heating cycles (for details see Sterner et al., 1988). In some inclusions only KCl crystals were observed, and sylvite melted in the absence of halite. However, in other inclusions of the same populations, sudden halite precipitation on the dissolving sylvite crystal was observed just before sylvite dissolved. It was therefore concluded that in halite-absent inclusions, halite failed to precipitate when the composition of the liquid crossed the cotectic line between the KCl and NaCl field (Fig. 4A) at temperatures lower than about 100 °C. These inclusions have been omitted in Figure 4. In B33, the KCl contents in the weakly saline region are also uncertain and may be very low, since KCl melting temperatures could not be measured in the presence of hydrohalite or ice (Fig. 4B). Final melting of hydrohalite was not observed in the presence of sylvite or ice. Apparent initial melting in most inclusions occurred at −50 to −32 °C, indicating that $CaCl_2$ or $MgCl_2$ were present (Crawford, 1981).

Bulk leachate analyses of all samples resulted in significant Mg^{2+} and Ca^{2+} contents (Table 2). Because of the poor reproducibility of replicates, the determined Ca/Na ratios are ambiguous. If contamination by solid calcite inclusions is assumed to account for the high values of B502/2 and B33/1 (Table 2) it would seem that the actual Ca/Na ratios were low at values of around 0.2 (B502) and 0.06 (B33). Mg/Na ratios are in the range of 0.1 in both samples. Thus, the NaCl and KCl contents estimated from the microthermometric data using Figure 4A and 4B are

too high (Sterner et al., 1988), and the total salinities were classified as apparent. However, it remains unclear whether the Ca/Na and Mg/Na ratios remained constant throughout the populations or whether a correlation with the total salinities exists like that detected for the K/Na ratios.

During the freezing and heating cycles, no phase transitions could be detected in the vapor bubbles of the H_2O-rich highly saline inclusions. Formation and melting of clathrates could not be observed. The vapor bubbles in the inclusions of samples B503 and B504 consist of pure CH_4, as confirmed by Raman spectroscopy.

Homogenization temperatures to liquid cover a wide temperature range from 150 to 573 °C (Fig. 5A, 5B). Nevertheless, the range of T_h(V → L) of each population does not exceed ±10 °C. From 150 to 380 °C, T_h(V → L) of all inclusions is equal to the last salt melting temperature, corresponding to 33–66 wt% $(KCl + NaCl)_{eq}$ in samples B502 and B503. This indicates that the fluid populations at this temperature range were salt-saturated. There are no inclusions in which T_m(salts) is significantly higher than T_h(V → L). This suggests that heterogeneous trapping of salt-saturated fluids with precipitated salt crystals did not occur. This is unlike developments in many other hydrothermal and contact-metamorphic fluid systems (e.g., Ahmad and Rose, 1980; Williams-Jones and Ferreira, 1989; Kelley and Robinson, 1990). In samples B502 and B503, fluid populations with T_h(V → L) from 400 to 580 °C were salt-undersaturated and displayed relatively constant salinities from 67 to 73 wt% $(NaCl + KCl)_{eq}$. At this T range, apparent total salinities are not correlated with T_h(V → L). Above 500 °C, many inclusions decrepitated before homogenization occurred, and none of them survived the transition from α to β quartz. Apparent KCl/(KCl + NaCl) ratios correlate significantly with the total homogenization temperatures. Recalculated apparent K/Na ion ratios in samples B502 and B503 have maximum values of 1.75 and 1.80 at T_h(V → L) of 500–573 °C down to minimum values of about 0.3 at T_h = 150 °C. This is also true of sample B33, in which the apparent KCl content and the total salinities are lower (Fig. 4B) and the apparent K/Na ratios shift to lower maximum values of 0.8 at T_h(V → L) = 450–530 °C down to ≤0.13 at T_h(V → L) = 95 °C. It is evident that the K/Na ion ratio decreases at least half an order of magnitude in all samples as T_h(V → L) decreases from maximum to minimum values.

Vapor-rich CO_2-bearing inclusions. These inclusions are exclusively associated with highly saline inclusions having $T_h \geq 500$ °C. Melting of solid CO_2 could be observed only in 13 out of 60 inclusions from both B502 and B33. $T_m(CO_2)$ ranges from −56.3 to −57.1 °C, indicative of pure CO_2. The amount of liquid produced near the CO_2 triple point is estimated to be 10–15 vol%, which is just above the optical resolution for a liquid film around a vapor bubble. CO_2 homogenized to the vapor phase. The apparent T_hCO_2(L → V) range from about −50 to a maximum value of 0 °C. If the optical resolution for the last visible liquid is assumed to be 10 vol%, the true T_h(L → V) are higher. Using the curves of Walther (1981) relating temperature and volume, the apparent T_h(L → V) of 0 °C corresponds to the true value of +18°, corresponding to the maximum density of 0.18 g/cm³ for the CO_2 system (Kerrick and Jacobs, 1981). The mean value of 0.14 ± 0.04 g/cm³ covers all observed T_hCO_2(L → V). The amount of the aqueous phase is estimated to be 5–10 vol% at room temperature. Owing to the small amounts of the liquid, final ice melting in the presence of clathrate was observed in only 17 inclusions. T_m ice ranges between −4.1 and −10.5 °C, corresponding to salinities of 6–14.5 wt% $NaCl_{eq}$ (Potter et al., 1978). Clathrate melting was observed in a few inclusions, and the corresponding salinities are broadly coincident with those derived from T_m ice. H_2O-CO_2 homogenization occurred to vapor. The apparent T_hH_2O-CO_2(L → V) were preferentially estimated in inclusions with reentrants and range from 350 to 460 °C. Due to difficulties in observing the final disappearance of liquid, these estimates are likely to be too low with true T_h(L → V) at least 100 °C higher. Thus, the homogenization temperatures of the vapor-rich CO_2-bearing inclusions broadly coincide with the peak homogenization temperatures of the highly saline inclusions associated with them. Estimates for the bulk inclusion density depend on the amount of the aqueous phase at the inclusion walls. On the basis of liquid-vapor ratios and values of phase densities from Parry (1986) and Brown (1989), the vapor-rich CO_2-bearing inclusions have bulk densities of 0.23 ± 0.04 g/cm³ and contain between 35 and 55 mol% CO_2 and 1–3 mol% $NaCl_{eq}$.

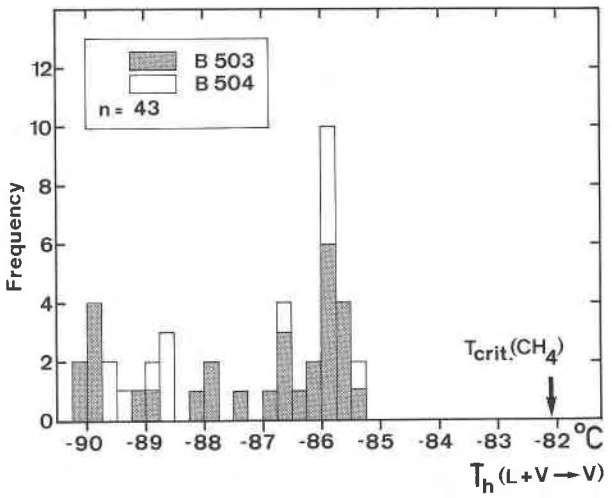

Fig. 6. Histogram illustrating the apparent homogenization temperatures to the vapor phase of the methane system of methane-bearing inclusions in graphite-containing metacherts B503 and B504.

Vapor-rich CH_4-bearing inclusions. In these inclusions, methane homogenized to vapor between −85 and −90 °C (Fig. 6). The densities for the CH_4 system are 0.08 ± 0.02 g/cm³, as derived from Jacobs and Kerrick (1981).

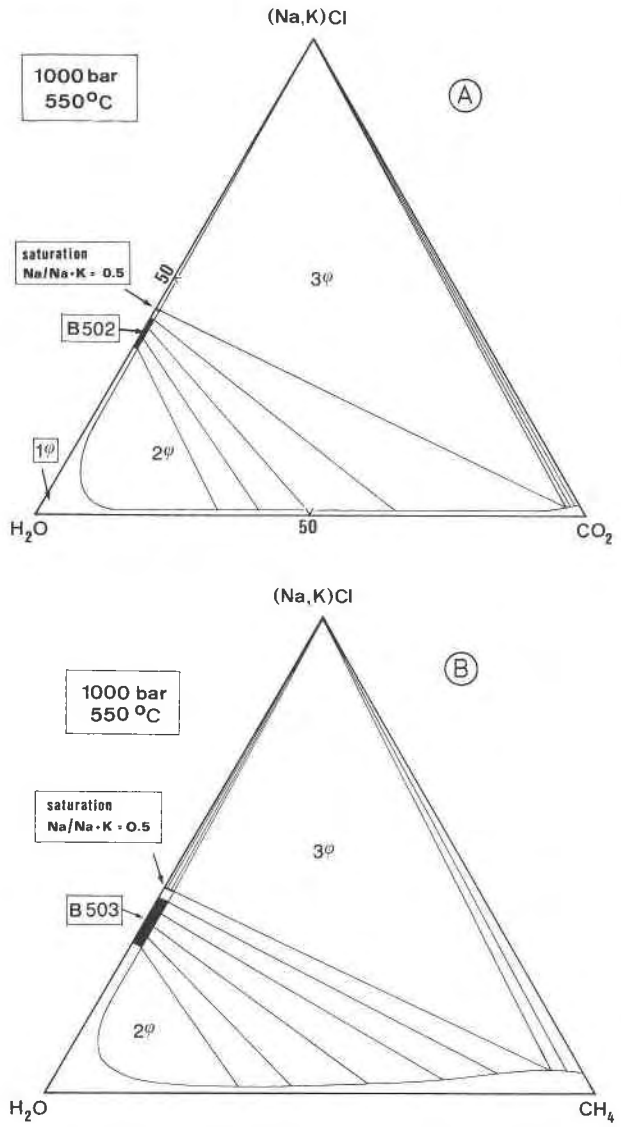

Fig. 7. (**A**) Schematic isobaric isothermal section of the system H_2O-CO_2-(Na,K)Cl at 1000 bars and 550 °C (mol%) exhibiting the two-fluid immiscibility field, based on experimental data of Frantz et al. (1992). The diagram is tentatively extrapolated to high salinities, at which the exact position of the phase boundaries is not known. Data for salt saturation on the H_2O-rich side are from Sterner et al. (1988). (**B**) Schematic isothermal section of the system H_2O-CH_4-(Na,KCl) at 550 °C and 1000 bars, based on experimental work by Krader (1985) and tentatively extrapolated to high salinities (see above).

Raman spectrometry showed that the vapor phase is pure CH_4. The spectral position of ν_1 (CH_4) of some inclusions is at 2914.1 cm^{-1}. Applying the calibration curve of Chou et al. (1990) for the position of ν_1 as a function of pressure resulted in an internal CH_4 pressure of about 110 bars at room temperature. Using the equation of state of Jacobs and Kerrick (1981), this corresponds to a CH_4 density of 0.089 g/cm^3, well within the range detected by microthermometry. Melting of clathrate was not observed. The amount of aqueous liquid is estimated to be <10 vol%. Total homogenization temperatures into the vapor phase are estimated to range from 250 to 500 °C. The salinity of the aqueous phase is highly variable. In many inclusions, such as that shown in Figure 3D, one or more salt crystals are present. Melting of salt did not occur by heating up to 600 °C, indicating that this fluid was trapped in the presence of precipitated salt crystals. Bulk densities are estimated to be 0.15 ± 0.04 g/cm^3, depending chiefly on the estimated amount and salinity of the aqueous phase. With the assumption of 5–10 vol% H_2O, the inclusions contain between 40 and 65 mol% CH_4.

Discussion

Fluid immiscibility

Textural relationships suggest that highly saline H_2O-rich inclusions and vapor-rich CO_2- and CH_4-bearing inclusions were simultaneously trapped in the solvus of the H_2O-CO_2-salt and H_2O-CH_4-salt systems. To verify this interpretation with microthermometric data one must demonstrate that (1) each group displays contrasting homogenization modes (L + V → L; L + V → V), (2) total homogenization temperatures are coincident for each group, and (3) compositions and bulk densities fit into experimentally determined solvi in the model systems. The homogenization temperatures and pressures of the two immiscible fluids then approximate their entrapment conditions (Pichavant et al., 1982; Ramboz et al., 1982; Bottrell et al., 1990). Given that the vapor-rich CO_2-bearing inclusions are associated only with highly saline brines of $T_h \geq 500$ °C and that the true T_h of CO_2-rich inclusions may exceed the apparent values of 350–460 °C by >100 °C (Walther, 1981), the data clearly meet requirements 1 and 2. This supports the textural evidence and indicates that in samples B502 and B33 two immiscible fluids have been trapped at temperatures of 500 to at least 573 °C at the wollastonite isograd. There is no evidence for trapping of vapor-rich CO_2-bearing inclusions at lower temperatures after the brine became salt-saturated. In samples B503 and B504 two immiscible fluids in the H_2O-CH_4-salt ternary have been trapped in similar conditions. In the latter case, estimated homogenization temperatures as low as 250 °C for the vapor-rich inclusions and the presence of salt crystals in them indicate that trapping of two coexisting fluids occurred under salt-saturated conditions.

Experimentally determined data on the solvus of the H_2O-CO_2-NaCl system are available up to salinities of about 50 wt% of the brine (Frantz et al., 1992). In the system H_2O-CH_4-NaCl, data are only available up to 8 wt% NaCl (Krader, 1985). Figure 7 shows schematic isobaric isothermal sections of these systems at a temperature of 550 °C and 1000 bars tentatively extrapolated to (Na,K)Cl contents of 65–73 wt%. Although the position of the phase boundaries and the tie lines is not exactly known, it is evident that H_2O-rich highly saline brines

coexist with low-density CO_2-rich vapors containing a few mole percent of salts (Pichavant et al., 1982). The estimated contents in vapor-rich inclusions of between 35 and 55 mol% CO_2 (B502 and B33) and between 40 and 65 mol% CH_4 (B503 and B504) are compatible with the schematic phase diagrams. Isochores for vapor-rich inclusions were calculated using the *PVT* data computed by Brown (1989). The estimated bulk densities and compositions for the CO_2 inclusions correspond to internal pressures of 550–950 bars at 550 °C. Using corresponding densities and compositions of the vapor-rich CH_4-bearing inclusions of samples B503 and B504 and applying graphical interpolations from Krader's (1985) experimental data, internal pressures of 480–990 bars are estimated. Hence, the maximum values of the estimated pressures in both systems also agree with the interpretation of simultaneous trapping on the two-fluid solvi. The high internal pressures may account for the frequent decrepitation of hypersaline brine inclusions before homogenization at temperatures above 500 °C. Given that sedimentary cover during the Oligocene was at least 2000 m and not more than 3000 m (Ramirez-Fernandez and Heinrich, 1991), fluid pressure was nearly lithostatic and certainly not hydrostatic.

T-X conditions of the formation of wollastonite rims

It has been shown that aqueous fluids trapped in the metacherts are represented by highly saline brines and that vapor-rich CO_2-bearing inclusions are associated only with brines trapped above 500 °C. Weakly saline fluids are absent. The formation of wollastonite rims must therefore have taken place at the H_2O-rich side of the solvus for the H_2O-CO_2-salt system. This occurred at temperatures given by the intersection point of the wollastonite-producing reaction with the two-fluid solvus or above (Fig. 8). At 1000 bars and up to 35 wt% NaCl, these isobaric invariant points always lie above 500 °C at distinct X_{CO_2} values, and it is most likely that this is also valid for very high salinities (Fig. 8). If one accepts the tentative extrapolation up to 70 wt% (shaded area in Fig. 8), that would mean that wollastonite could have formed at temperatures at the solvus of >600 to about 500 °C at X_{CO_2} of about 0.02. These temperatures coincide with the temperatures at which the trapping of the two immiscible fluids occurred. This strongly suggests that the immiscible vapor-rich CO_2-bearing fluid was generated in situ by the reaction calcite + quartz = wollastonite + CO_2. This is also supported by textural observations (Fig. 3C) and renders an interpretation of the CO_2 fluid as generated by exsolution from the brine during cooling as highly improbable. Trommsdorff and Skippen (1986) showed that whenever immiscible low-density CO_2-rich fluid is generated by a decarbonation reaction at the two-fluid solvus, it is preferentially removed from the system (see also Yardley and Bottrell, 1988). The result is vapor loss by boiling (Trommsdorff and Skippen, 1986). Large amounts of wollastonite + CO_2 can be produced at the solvus without increasing the X_{CO_2} of the brine. H_2O is transferred to a minor extent from the brine into the low-density H_2O-CO_2 fluid, and the salinity of the brine is increased.

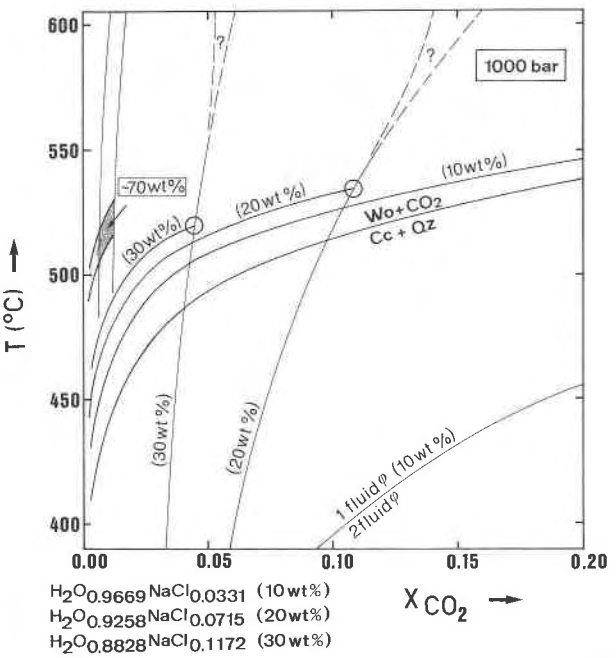

Fig. 8. Pseudobinary isobaric X_{CO_2}-T sections at 1000 bars and low X_{CO_2} illustrating the position of the reaction calcite + quartz = wollastonite + CO_2 relative to the two-fluid immiscibility field at various NaCl contents. The reaction curves were calculated using mineral data from GeO-Calc (Brown et al., 1988) along with f_{CO_2} values in the H_2O-CO_2-NaCl ternary from Bowers and Helgeson (1983b). The two fluid boundaries were graphically interpolated and extrapolated from Gehrig (1980) and Frantz et al. (1992). Circles denote maximum temperatures for fluid buffering by this reaction. The shaded area is a tentative extrapolation to salinities of ≈70 wt%.

As regards cooling below 500 °C, the fluid composition should leave the solvus and should, in principle, be buffered by the reaction of wollastonite + CO_2 to calcite + quartz (Fig. 8). The presence of inner calcite rims between the remaining quartz nodules and the wollastonite rims (Fig. 2C) indicates that this back reaction occurred locally. However, fluid inclusion characteristics indicate that the fluid composition was not buffered during cooling and that it did follow the two-fluid solvus down to low temperatures. The concomitant formation of pectolite rims during cooling (Fig. 2C) by the reaction wollastonite + HCl + $NaCl_{aq}$ = pectolite + $CaCl_{2\,aq}$ might have prevented retrograde fluid buffering.

Brine infiltration along metacherts

Within the marbles, the frequent occurrence of isobaric univariant and invariant assemblages suggests that the massive limestones formed a closed or nearly closed system with respect to the fluid phase and that fluid composition was internally buffered (Rice, 1977; Rice and Ferry, 1982), at least in the tremolite and diopside zones.

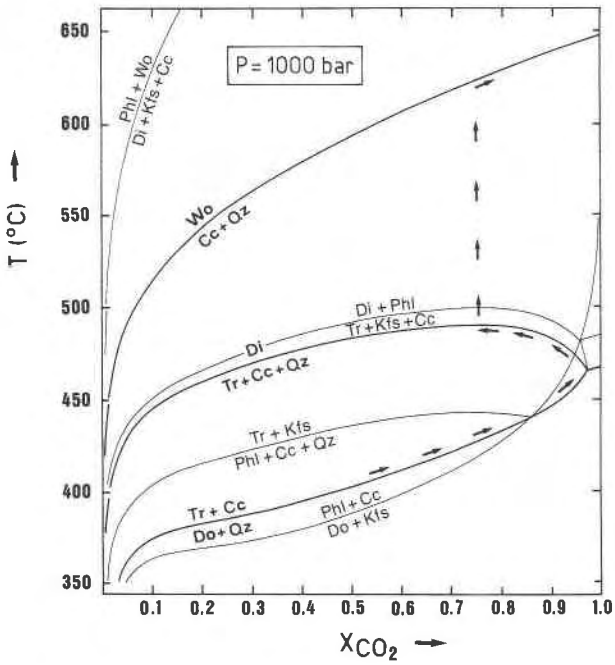

Fig. 9. Isobaric (P = 1000 bars) temperature-fluid composition diagram for tremolite-, diopside-, and wollastonite-producing reactions in the massive marbles (Tr = tremolite, Di = diopside, Wo = wollastonite, Cc = calcite, Do = dolomite, Qz = quartz, Kfs = alkali feldspar, Phl = phlogopite). Reactions involving Kfs and Phl contribute only to a minor extent to the formation of the index minerals and fluid evolution, respectively. Reaction curves are calculated for pure end-member compositions of the minerals using GeO-Calc (Brown et al., 1988). The arrows indicate the X_{CO_2}-T evolution in a closed system.

Figure 9 shows an isobaric T-X_{CO_2} section in the system CaO-MgO-SiO_2-H_2O-CO_2 for tremolite-, diopside-, and wollastonite-producing reactions at 1000 bars, as estimated by maximum densities of vapor-rich fluid inclusions. Depending on the composition of the fluid, the first occurrence of tremolite occurs at approximately 350–400 °C. With the assumption of a limiting case of a completely closed system, the buffering capacity of the system sets the first occurrence of diopside at 460 °C and $X_{CO_2} = 0.9$, the last occurrence of tremolite at 490 °C and $X_{CO_2} = 0.75$, and the first occurrence of wollastonite at 610 °C and $X_{CO_2} = 0.75$. Figure 9 also shows tremolite- and diopside-producing reactions involving alkali feldspar and phlogopite. Since bulk composition of the limestones are low in K_2O and Al_2O_3, these minerals are rare; therefore, they were not included in Figure 1.

At the diopside isograd, the isobaric invariant assemblage calcite + dolomite + quartz + tremolite + diopside fixes T and X_{CO_2} in marbles at about 470 °C and 0.9. Wollastonite rims indicate that in metacherts X_{CO_2} was ≤ 0.02, irrespective of whether immiscibility occurred (Figs. 8, 9). Sharp boundaries between wollastonite rims and marbles indicate that such large X_{CO_2} gradients occurred along distances of a few centimeters across the boundary between the wollastonite rim and the marble. The absence of wollastonite in diopside-zone marbles shows that similar gradients existed also throughout the diopside zone. It is clear that a different fluid regime controlled the metamorphic evolution of the metachert layers from that which prevailed in the limestones. Wollastonite rims along chert layers in the diopside and tremolite zones require infiltration of H_2O-rich fluids, thus maintaining low X_{CO_2} and enhancing the decarbonation reaction, which in its turn is enhanced by fluid immiscibility. The metacherts acted as channelways for the brines. Limestones of the tremolite and diopside zones were impervious for highly saline fluids. Infiltration of even very small amounts of brines into the marbles must be excluded, since that would have resulted in substantial progress of the reaction calcite + quartz = wollastonite + CO_2 in the marbles at the H_2O-rich side of the two-fluid solvus (Trommsdorff and Skippen, 1986). Phase equilibria considerations are not conclusive as to whether the wollastonite-zone marbles were subject to brine infiltration. However, stable isotope studies indicate that brine infiltration was confined to a zone 7–17 m wide closely adjacent to the intrusive contact (Heinrich and Hubberten, in preparation).

The peak temperature at the wollastonite isograd was 610 °C at 1000 bars when derived from the wollastonite-producing reaction in a closed marble system (Fig. 9). Temperatures of 560–585 ± 30 °C result when using thermometry of the univariant assemblage garnet + quartz + plagioclase + wollastonite in neighboring metaargillite lenses (Heinrich and Gottschalk, in preparation). Given the pressure uncertainty from fluid inclusion densities, these temperatures broadly coincide. That fluid inclusion samples from the wollastonite isograd have maximum homogenization temperatures of at least 573 °C implies that trapping of two immiscible fluids in the metacherts actually started at peak metamorphic conditions of about 600 °C and continued during cooling down to about 500 °C.

Infiltration and K-Na metasomatism are further confirmed by the presence of pectolite and potassium richterite in the previously alkali-poor metachert protolith. The formation of potassium richterite at the expense of diopside indicates that brine infiltration did not set in before peak metamorphic conditions were achieved at the wollastonite isograd.

Origin and history of brines

The hypersaline brine populations, along with the vapor-rich CO_2-bearing inclusions, represent the earliest fluids detectable in the metachert system at the wollastonite isograd. Although hypersaline, their salt-undersaturated nature at high T_h(V → L) implies that they have not been derived from boiling of salt-saturated weakly saline fluid (Ramboz et al., 1982). The hypersaline brines of 66–73 wt% $(NaCl + KCl)_{eq}$ and K/Na ion ratios of approximately 1 are therefore interpreted as having infiltrated as a fluid phase emanating from the crystallizing intrusion. The absence of a vertical fluid system, com-

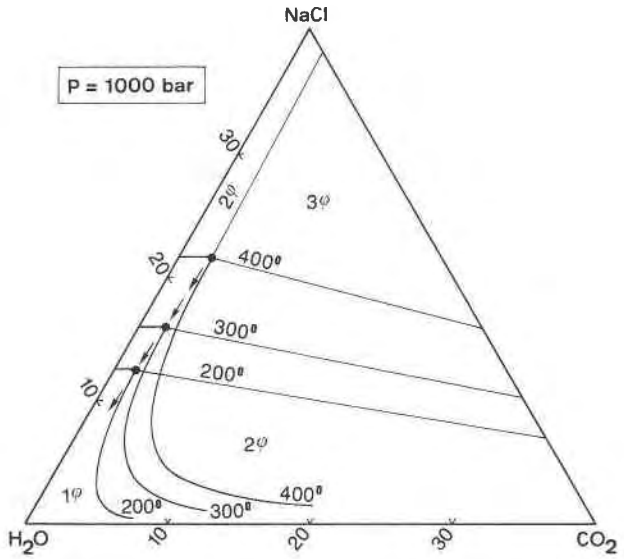

Fig. 10. Isobaric isothermal section of the H_2O-rich part of the system H_2O-CO_2-NaCl at 1000 bars exhibiting the compositions of salt-saturated brines (solid circles) coexisting with CO_2-rich vapor at various temperatures. The arrows indicate the evolution of the brine during isobaric cooling from 400 to 200 °C. Data for the two-fluid solvus extrapolated from Gehrig (1980); salt saturation in the H_2O-NaCl binary from Sterner et al. (1988).

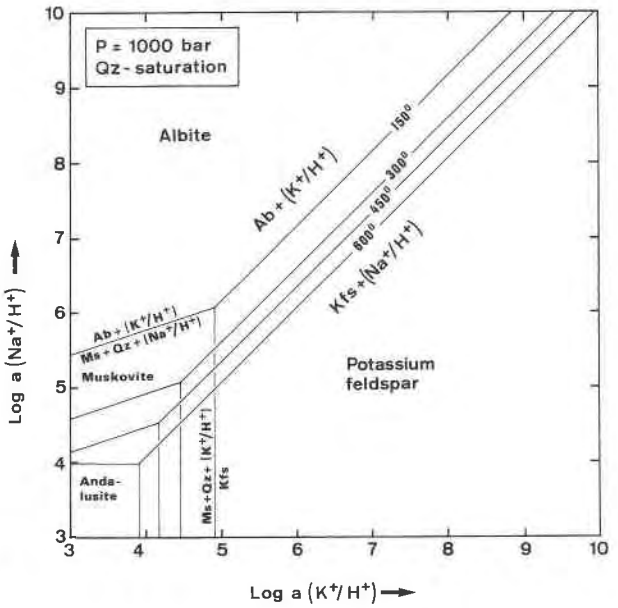

Fig. 11. Logarithmic activity diagram for a portion of the system Na_2O-K_2O-Al_2O_3-SiO_2-HCl at various temperatures for P = 1000 bars and at quartz saturation. The position of the stability field boundaries were computed using Ge0-Calc (Brown et al., 1988).

bined with evidence for lithostatic pressure implies that this fluid was exsolved directly from the magma as a hypersaline brine and does not represent a condensate (e.g., Hein and Tistl, 1987). Decarbonation occurred and, as a result of immiscibility, the low-density CO_2-bearing fluid might have left the system. This implies that the original brine might have been less saline. The extent of this modification would depend on the extent of the wollastonite-producing reaction.

The infiltrated brines did not escape into the marbles. One can reasonably infer that the brine in the metachert layers shared the same cooling history as the aureole. If trapping had occurred continuously during cooling, brine inclusions would have evolved toward lower T_h(V → L) at constant salinities along the H_2O-CO_2-salt solvus until salt saturation had been attained. Then salinities would have decreased, as would T_h(V → L), until $T_h = T_m$(salt). That should precipitate salt. Figure 5A shows precisely such a fluid evolution, indicating that the cooling brines attained salt saturation at 350–400 °C and that trapping actually occurred continuously throughout the cooling history down to 150 °C. Inclusions of solid halite or sylvite were not observed. It follows from the simplified H_2O-CO_2-NaCl system (Fig. 10) that the CO_2 content of the salt-saturated brine is only slightly reduced during cooling from 400 to 150 °C. Only small amounts of CO_2 were therefore exsolved. That may explain the absence of vapor-rich CO_2-bearing inclusions at temperatures below 500 °C. CO_2-rich fluids were trapped, obviously, only at temperatures above that for the decarbonation reaction.

If this interpretation is correct, the brines in the metachert system must have been in contact with the large fluid reservoir of the cooling alkali syenite, and reequilibration processes must have occurred, at least partially (Labotka et al., 1988). The composition of this fluid reservoir is controlled by the mineralogy of the alkali syenite, which consists of about 90% of the mode of perthitic alkali feldspar and is quartz-normative (Ramirez-Fernandez and Heinrich, 1991). Thus, under quartz-saturated conditions, the activities of Na^+ and K^+ in the fluid coexisting with the feldspars are approximated by the equilibrium potassic feldspar + Na^+/H^+ = albite + K^+/H^+, which is highly dependent on temperature (Fig. 11). The ratio of a_{K^+}/a_{Na^+} is about 1 at 600 °C and decreases about one order of magnitude when the temperature drops to 150 °C. The actual activity coefficients are unknown, but it is clear that the alkali concentrations in terms of K/Na ion ratios should broadly follow the same trend. As shown above, this trend is clearly seen in the evolution of the brines. It is therefore concluded that a continuous outflow of fluids in equilibrium with the intrusion occurred along the metachert channels down to 150 °C. Their compositional characteristics, unless somewhat modified by the loss of CO_2-rich vapor during the process of decarbonation, were mainly controlled by mineral-fluid equilibria in the cooling intrusion.

Direction of brine flow

Ferry (1991), Baumgartner and Ferry (1991), and Ferry and Dipple (1992) argued that the channelized flow of

aqueous fluids in the direction of decreasing temperature under equilibrium conditions would produce a sharp reaction front at a single temperature and a single field point. In Bufa del Diente metacherts then, a band completely reacted to wollastonite would change abruptly into quartzite without wollastonite rims at some distance from the contact. In contrast, brine flow in the direction of increasing temperature would generate a wide zone in which calcite + quartz + wollastonite would coexist. Their arguments hold, even if immiscibility occurs. As shown above, both features are not observed in the Bufa del Diente metacherts.

Wollastonite rims along metachert bands clearly represent nonequilibrium textures (see Joesten, 1991). That implies that equilibrium between calcite + quartz + wollastonite and infiltrating brines was not maintained over a few centimeters once wollastonite rims had formed. It can reasonably be inferred that the thin pegmatitic veinlets (Fig. 2B) trace the path of the infiltrating fluid. These indicate that flow occurred exclusively in the quartzite layers and not in the developing wollastonite rims. The decarbonation reaction progress at any point is then controlled by a complex interplay of mass transport through the already developed wollastonite rim. This may enhance in situ wollastonite formation. On the other hand, the advancing brine flow would cause wollastonite production with decreasing temperature away from the contact. Hydrothermal experiments (e.g., Tanner et al., 1985; Heinrich et al., 1989; Lüttge and Metz, 1992) have shown that mass transport through calc-silicate-armored relics is a very slow process and may well be slower than hydrous fluid fluxes under contact or regional metamorphic conditions (Labotka et al., 1988; Baumgartner and Ferry, 1991). Thus, the interpretation of the flow of the infiltrating brines in the direction of decreasing temperature is compatible with the observed textures, as well as with the occurrence of wollastonite formation from peak metamorphism of about 600 down to about 500 °C.

Two-fluid flow in the aureole

Infiltration of highly saline brine was confined to the metachert layers, and immiscibility of CO_2-bearing fluid produced by decarbonation occurred within the metachert layers. The low-density CO_2-rich fluid must then have infiltrated into overlying marble. This idea is supported by observations made by Yardley and Bottrell (1988), who argued that where two immiscible fluid phases coexist, the one produced by reaction tends to move out of the rock and leave the other behind. The rarity of phenomena such as shown in Figure 3B confirms that immiscible fluids, in general, move separately (Yardley and Bottrell, 1988). Experiments by Holness and Graham (1991) have shown that the fluid phase topology in marbles is a connected network for fluid only with X_{CO_2} close to 0.5, permitting grain-edge flow in marbles only for such fluid compositions. Holness and Graham (1991) concluded "marbles would be impervious to the infiltration of H_2O-rich fluids and could therefore act as a semipermeable membrane losing locally generated fluid, but excluding infiltrating fluid." This describes perfectly what happened at the metachert-marble boundaries at the Bufa del Diente aureole. In contrast, quartz-dominated lithologies permit pervasive flow of H_2O-NaCl fluids, but not of H_2O-CO_2 fluids (Watson and Brenan, 1987; Holness and Graham, 1991). Vertical transport of immiscible low-density CO_2-bearing fluid at the Bufa del Diente aureole was further confirmed by stable isotope studies (Heinrich and Hubberten, 1991, and in preparation). Relative changes in C and O isotopes along short profiles in overlying, silicate-free marble perpendicular to the wollastonite-rimmed metachert layers at the wollastonite zone indicated that the fluid causing isotopic alteration in the marble was CO_2-rich.

If so, simple mass balance calculations will estimate the amount of low-density CO_2-rich fluid generated at the chert-marble boundary that subsequently infiltrated the overlying marble. If one assumes that all low-density CO_2-rich fluid is immediately lost, and one assumes an average fluid composition of $X_{CO_2} = 0.5$, $X_{CO_2} = 0.47$, and $X_{NaCl_{eq}} = 0.03$ and an average density of 0.25 g/cm^3 at 550 °C, every cubic centimeter of wollastonite produced corresponds to approximately 6 cm^3 CO_2-rich fluid infiltrating the overlying marble. Given the average wollastonite rim thickness at the wollastonite isograd, the central diopside zone, and the diopside isograd, and taking the values for fluid composition and density from above into account along with the mean thickness of the Cuesta del Cura Formation with about 50 chert layers, one finds that about 900, 600, and 90 cm^3, respectively, of CO_2-rich fluid infiltrated a marble column 1 cm × 1 cm × 70 m at the three outcrops B502, A17, and B4 (Fig. 1). With the fluid flow distributed homogeneously along the whole column, this would correspond to volumetric fluid-rock ratios of 0.13, 0.08, and 0.013. Thus, less CO_2 infiltrated the marbles than was produced by them internally (Fig. 9).

A striking point is that there is no indication of mixing between low-density CO_2 and CH_4 fluids. In graphite-free metacherts, C must have been removed, probably by loss of CH_4-rich fluid. However, the CO_2-rich inclusions measured in B502 and B33 are CH_4-free. On the other hand, the metacherts B503 and B504 do contain CH_4 fluids coexisting with graphite, which are CO_2-free despite the fact that thick wollastonite rims indicate that large amounts of CO_2 had been produced. A reasonable suggestion is that the two fluids never coexisted. Since the wollastonite-producing reaction follows a dissolution-precipitation mechanism (Tanner et al., 1985; Kerrick et al., 1991), CO_2 must have been generated at the dissolving calcite crystals at the calcite-wollastonite boundaries. Fluid loss probably occurred immediately. In contrast, the fluid inclusion characteristics suggest that CH_4 formation by reaction of the brines with the C inside the quartzite nodules was sluggish and occurred over a wide time-temperature range. Removal of CH_4-rich fluid might have been hindered by lack of grain boundary wetting by

CH_4 in the quartzite matrix. If so, persistence of a separate CH_4-rich fluid in the quartzite possibly inhibited rapid breakdown of graphite (see also Yardley and Bottrell, 1988).

Concluding remarks

It has been shown that the limestones of the Cuesta del Cura Formation acted as aquitards and prevented formation of convection cells of hydrous fluids, as are commonly observed in silicate-rich country rocks around shallow intrusions (Barton et al., 1991). Limestones are impervious to grain-edge flow of aqueous fluids and quartz-rich beds of CO_2-rich fluids (Watson and Brenan, 1987; Holness and Graham, 1991). Whenever a fracture system in an aureole is absent, convection cells cannot build up in metasediments containing specific stratigraphic horizons of these different lithologic types, no matter which fluid type is present. Vertical fluid transport on a large scale in interstratified sediments is only possible by fracturing. Fracturing processes induced by emplacement tectonics play an important role in the roof pendants of intrusions (Paterson et al., 1991; Barton et al., 1991). At the Bufa del Diente aureole, fracturing was observed in marbles of the Tamaulipas Formations south of the intrusion that were lifted to a much higher level during emplacement. The vast majority of aqueous fluid released by the alkali syenite may have escaped by this mechanism.

Experimental work by Johnson (1991) showed that the immiscibiltiy field in the H_2O-CO_2-salt system expands rapidly with pressure and that immiscibility occurs at granulite facies conditions even at moderate salinities. Johnson (1991) pointed out that fluid immiscibility is a widespread phenomenon in metamorphic rocks. Thus, in calcareous metasediments, boiling off of CO_2-rich fluid produced by decarbonation reactions at the two-fluid solvus may cause contrasting fluid flow patterns over a wide range of P-T conditions up to the granulite facies.

Acknowledgments

I thank the members of the Facultad de Ciencias de la Tierra, Universidad Autónoma de Nuevo León, Linares, México, for field assistance. P. Metz and D. Mangliers, Mineralogisch-Petrographisches Institut, Universität Tübingen, and F. Galbert, ZELMI, Technische Universität Berlin, provided electron microprobe facilities. Thanks go also to A. Becker, SFB 69, Technische Universität Berlin, who performed AAS and ICP analyses, and to E. Horn, IGDL, Universität Göttingen, for help with the Raman analysis. M. Gottschalk, F. Lucassen, and A. Lüttge read earlier versions of the manuscript. Very constructive reviews of V. Sisson and W. Lamb improved the paper substantially. Part of this work was supported by a research grant of the Mexican Secretaría de Educación Pública.

References Cited

Ahmad, S.N., and Rose, A.W. (1980) Fluid inclusions in porphyry and skarn ore at Santa Rita, New Mexico. Economic Geology, 75, 229–250.

Barton, M.D., Staude, J.M., Snow, E.A., and Johnson, D.A. (1991) Aureole systematics. In Mineralogical Society of America Reviews in Mineralogy, 26, 723–847.

Baumgartner, L.P., and Ferry, J.M. (1991) A model for coupled fluid-flow and mixed-volatile mineral reactions with applications to regional metamorphism. Contributions to Mineralogy and Petrology, 106, 273–285.

Bottrell, S.H., Greenwood, P.B., Yardley, B.W.D., Shepherd, T.J., and Spiro, B. (1990) Metamorphic and post-metamorphic fluid flow in the low-grade metamorphic rocks of the Harlech dome, north Wales. Journal of Metamorphic Geology, 8, 131–143.

Bowers, T.S., and Helgeson, H.C. (1983a) Calculation of the thermodynamic and geochemical consequences of nonideal mixing in the system H_2O-CO_2-NaCl on phase relations in geological systems: Metamorphic equilibria at high pressures and temperatures. American Mineralogist, 68, 1059–1075.

——— (1983b) Calculation of the thermodynamic and geochemical consequences of nonideal mixing in the system H_2O-CO_2-NaCl on phase relations in geologic systems: Equation of state for H_2O-CO_2-NaCl fluids at high pressures and temperatures. Geochimica et Cosmochimica Acta, 47, 1247–1275.

Brown, P.E. (1989) FLINCOR: A microcomputer program for the reduction and investigation of fluid-inclusion data. American Mineralogist, 74, 1390–1393.

Brown, T.H., Berman, R.G., and Perkins, E.H. (1988) Ge0-Calc: Software package for calculation and display of pressure-temperature-composition phase diagrams using an IBM or compatible personal computer. Computers and Geosciences, 14, 279–289.

Chou, I.-M., Pasteris, J.D., and Seitz, J.C. (1990) High-density volatiles in the system C-O-H-N for the calibration of a laser Raman microprobe. Geochimica et Cosmochimica Acta, 54, 535–543.

Crawford, M.L. (1981) Phase equilibria in aqueous inclusions. In L.S. Hollister and M.L. Crawford, Eds., Short course in fluid inclusions: Applications to petrology, p. 75–100. Mineralogical Association of Canada, Toronto, Ontario, Canada.

Ferry, J.M. (1983) Applications of the reaction progress variable in metamorphic petrology. Journal of Petrology, 24, 343–376.

——— (1986) Reaction progress: A monitor of fluid-rock interaction during metamorphic and hydrothermal events. In J.V. Walther and B.J. Wood, Eds., Fluid-rock interactions during metamorphism, p. 60–88. Springer-Verlag, New York.

——— (1987) Metamorphic hydrology at 13-km depth and 400–550 °C. American Mineralogist, 72, 39–58.

——— (1988) Contrasting mechanisms of fluid flow through adjacent stratigraphic units during regional metamorphism, south-central Maine, USA. Contributions to Mineralogy and Petrology, 98, 1–12.

——— (1991) Dehydration and decarbonation reactions as a record of fluid infiltration. In Mineralogical Society of America Reviews in Mineralogy, 26, 351–393.

Ferry, J.M., and Dipple, G.M. (1992) Models for fluid flow, mineral reaction, and isotopic alteration during contact metamorphism: The Notch Peak aureole, Utah. American Mineralogist, 77, 577–591.

Frantz, J.D., Popp, R.K., and Hoering, T.C. (1992) The compositional limits of fluid immiscibility in the system H_2O-NaCl-CO_2 as determined with the use of synthetic fluid inclusions in conjunction with mass spectrometry. Chemical Geology, 98, 237–255.

Gehrig, M. (1980) Phasengleichgewichte und PVT-Daten ternärer Mischungen aus Wasser, Kohlendioxid und Natriumchlorid bis 3 kbar und 550 °C. Hochschulverlag, Freiburg, Germany.

Hein, U.F., and Tistl, M. (1987) Characteristics of fluid inclusions in the porphyry copper deposit at La Granja, Peru. Chemical Geology, 61, 183–192.

Heinrich, W., and Hubberten, H.W. (1991) Infiltration, buffering, and immiscibility of NaCl-KCl-H_2O-CO_2 fluids at Bufa del Diente intrusion, NE-México: Fluid inclusion and isotope studies. Terra Abstracts, 3 (1), 438.

Heinrich, W., Metz, P., and Gottschalk, M. (1989) Experimental investigation of the kinetics of the reaction 1 tremolite + 11 dolomite = 8 forsterite + 13 calcite + 9 CO_2 + 1 H_2O. Contributions to Mineralogy and Petrology, 102, 163–173.

Holness, M.B., and Graham, C.M. (1991) Equilibrium dihedral angles in the system H_2O-CO_2-NaCl-calcite, and implications for fluid flow during metamorphism. Contributions to Mineralogy and Petrology, 108, 368–383.

Hover-Granath, V.C., Papike, J.J., and Labotka, T.C. (1983) The Notch

Peak contact metamorphic aureole, Utah: Petrology of the Big Horse Limestone Member of the Orr Formation. Geological Society of America Bulletin, 94, 889–906.

Hubberten, H.W. (1985) The Sierra de San Carlos, Tamaulipas: An igneous complex of the eastern Mexican Alkaline Province. Zentralblatt für Geologie und Paläontologie, Teil 1, Heft 9/10, 1183–1191.

Jacobs, G.K., and Kerrick, D.M. (1981) Methane: An equation of state with application to the ternary H_2O-CO_2-CH_4. Geochimica et Cosmochimica Acta, 45, 607–614.

Joesten, R.L. (1991) Kinetics of coarsening and diffusion-controlled mineral growth. In Mineralogical Society of America Reviews in Mineralogy, 26, 507–582.

Johnson, E.L. (1991) Experimentally determined limits for H_2O-CO_2-NaCl immiscibility in granulites. Geology, 19, 925–928.

Kelley, D.S., and Robinson, P.T. (1990) Development of a brine-dominated hydrothermal system at temperatures of 400–500 °C in the upper level plutonic sequence, Troodos ophiolite, Cyprus. Geochimica et Cosmochimica Acta, 54, 653–661.

Kerrick, D.M., and Jacobs, G.K. (1981) A modified Redlich-Kwong equation for H_2O, CO_2, and H_2O-CO_2 mixtures at elevated pressures and temperatures. American Journal of Science, 281, 735–767.

Kerrick, D.M., Lasaga, A.C., and Raeburn, S.P. (1991) Kinetics of heterogeneous reactions. In Mineralogical Society of America Reviews in Mineralogy, 26, 583–672.

Krader, T. (1985) Phasengleichgewichte und kritische Kurven des ternären Systems H_2O-CH_4-NaCl bis 250 MPa und 800 K. Ph.D. thesis, University of Karlsruhe, Karlsruhe, Germany.

Labotka, T.C., Nabelek, P.I., Papike, J.J. (1988) Fluid infiltration through the Big Horse Limestone in the Notch Peak contact-metamorphic aureole, Utah. Amerian Mineralogist, 73, 1302–1324.

Lüttge, A., and Metz, P. (1992) Mechanism and kinetics of the reaction: 1 dolomite + 2 quartz = 1 diopside + 2 CO_2 investigated by powder experiments. Canadian Mineralogist, 29, 803–821.

Nabelek, P.I., Labotka, T.C., O'Neil, J.R., and Papike, J.J. (1984) Contrasting fluid/rock interaction between the Notch Peak granitic intrusion and argillites and limestones in western Utah: Evidence from stable isotopes and phase assemblages. Contributions to Mineralogy and Petrology, 86, 25–34.

Parry, W.T. (1986) Estimation of X_{CO_2}, P, and fluid inclusion volume from fluid inclusion temperature measurements in the system NaCl-CO_2-H_2O. Economic Geology, 81, 1009–1013.

Paterson, S.R., Vernon, R.H., and Fowler, T.K. (1991) Aureole tectonics. In Mineralogical Society of America Reviews in Mineralogy, 26, 673–722.

Pichavant, M., Ramboz, C., and Weisbrod, A. (1982) Fluid immiscibility in natural processes: Use and misuse of fluid inclusion data. I. Phase equilibria analysis: A theoretical and geometrical approach. Chemical Geology, 37, 1–27.

Potter, R.W., II, Clynne, M.A., and Brown, D.L. (1978) Freezing point depression of aqueous sodium chloride solutions. Economic Geology, 73, 284–285.

Ramboz, C., Pichavant, M., and Weisbrod, A. (1982) Fluid immiscibility in natural processes: Use and misuse of fluid inclusion data. II. Interpretation of fluid inclusion data in terms of immiscibility. Chemical Geology, 37, 29–48.

Ramirez-Fernandez, J.A., and Heinrich, W. (1991) Geology of the Tertiary Bufa del Diente intrusion and its contact aureole, Sierra de San Carlos, Tamaulipas, México. Zentralblatt für Geologie und Paläontologie, 6, 1519–1531.

Rice, J.M. (1977) Progressive metamorphism of the impure dolomitic limestone in the Marysville aureole, Montana. American Journal of Science, 277, 1–24.

Rice, J.M., and Ferry, J.M. (1982) Buffering, infiltration, and the control of intensive variables during metamorphism. In Mineralogical Society of America Reviews in Mineralogy, 10, 263–326.

Rumble, D., III, Ferry, J.M., Hoering, T.C., and Boucot, A.J. (1982) Fluid flow during metamorphism at the Beaver Brook fossil locality, New Hampshire. American Journal of Science, 282, 886–919.

Sisson, V.B., Crawford, M.L., and Thompson, P.H. (1981) CO_2-brine immiscibility at high temperatures: Evidence from calcareous metasedimentary rocks. Contributions to Mineralogy and Petrology, 78, 371–378.

Sterner, S.M., Hall, D.L., and Bodnar, R.J. (1988) Synthetic fluid inclusions. V. Solubility relations in the system NaCl-KCl-H_2O under vapor-saturated conditions. Geochimica et Cosmochimica Acta, 52, 989–1005.

Tanner, S.B., Kerrick, D.M., and Lasaga, A.C. (1985) Experimental kinetic study of the reaction: Calcite + quartz = wollastonite + carbon dioxide, from 1 to 3 kilobars and 500° to 850 °C. American Journal of Science, 285, 577–620.

Trommsdorff, V., and Skippen, G. (1986) Vapour loss ("boiling") as a mechanism for fluid evolution in metamorphic rocks. Contributions to Mineralogy and Petrology, 94, 317–322.

Trommsdorff, V., Skippen, G., and Ulmer, P. (1985) Halite and sylvite as solid inclusions in high-grade metamorphic rocks. Contributions to Mineralogy and Petrology, 89, 24–29.

Walther, J. (1981) Fluide Einschlüsse im Apatit des Carbonatits vom Kaiserstuhl (Oberrheingraben): Ein Beitrag zur Interpretation der Carbonatitgenese. Ph.D. thesis, University of Karlsruhe, Karlsruhe, Germany.

Watson, E.B., and Brenan, J.M. (1987) Fluids in the lithosphere. I. Experimentally determined wetting characteristics of CO_2-H_2O fluids and their implications for fluid transport, host-rock physical properties, and fluid inclusion formation. Earth and Planetary Science Letters, 85, 497–515.

Williams-Jones, A.E., and Ferreira, D.R. (1989) Thermal metamorphism and H_2O-CO_2-NaCl immiscibility at Parapedia, Quebec: Evidence from fluid inclusions. Contributions to Mineralogy and Petrology, 102, 247–254.

Yardley, B.W.D., and Bottrell, S.H. (1988) Immiscible fluids in metamorphism: Implications of two-phase flow for reaction history. Geology, 16, 199–202.

Manuscript received May 4, 1992
Manuscript accepted March 5, 1993